Pollutant Dispersion Over Two-Dimensional Hilly Terrain

Hyun Goo Kim* and Choung Mook Lee**

(*Received April 3, 1997*)

Numerical prediction of the wind flow and pollutant dispersion over two-dimensional hilly terrain is presented. The wind tunnel experiments are conducted to validate the numerical results of the flow field. Measured mean velocity profiles, turbulence characteristics, and surface pressure distributions show good agreement with the numerical predictions. The hypothesis of Reynolds number independency for an atmospheric boundary-layer flow over aerodynamically rough terrain is numerically confirmed. The linear theory provides generally good prediction of speed-up characteristics for gently sloped low hills. The effect of two-dimensional double hills on the dispersion of pollutants from continuously or temporally released line source of different emission heights and locations is also investigated. The ground-level concentrations are considerably reduced as emission heights are increased. The variances of ground-level concentration with respect to time from a temporally released source are strongly influenced by the flow separation.

Key Words: Atmospheric Boundary Layer, Flow Separation, Speed-Up, Ground-Level -Concentration, Pollutant Dispersion

1. Introduction

In many cases, the sources of air pollution are located in hilly terrain which strongly influence the local flow field as well as cause significant changes in the dispersion characteristics due to flow separation, stagnation, impingement, upwash and downwash, *etc.* There have been numerous investigations conducted over two-and three-dimensional hills of various shapes to find the relations between the flow field under topographic influences and the dispersion characteristics.

Field experiments have serious limitations due to the immense cost and the difficulties in controlling the experimental conditions. Most of experiments have been carried out in laboratories using wind tunnel or towing tank. A few examples are the investigations of Arya *et al.* (1981, 1987), Ohba *et al.* (1990), Snyder *et al.* (1991), Gong (1991) and Crooks and Ramsay (1993). Numerical investigations have been conducted, for instances, by Mouzakis and Bergeles (1991), Glekas and Bergeles (1994), and Ma and Robson (1995).

Numerical methods have many advantages in the simulation of air pollution scenarios. They are faster, less expensive and more reliable compared with the experiments. The dispersion scenarios of radioactive pollutants due to the failure of a nuclear power plant should be considered for all possible situations for a quick and proper countermeasure. The numerical models are regarded as more suitable tool for such a purpose.

In the present investigation, a numerical method for the prediction of pollutant dispersion into turbulent flow field over two-dimensional hilly terrain is presented. For a validation purpose, an associated experiment of the flow field is carried out in a wind tunnel.

* Advanced Fluids Engineering Research Center, Pohang University of Science & Technology, San 31 Hyoja-Dong, 790-784, Pohang, Korea

** Professor, Department of Mechanical Engineering, POSTECH

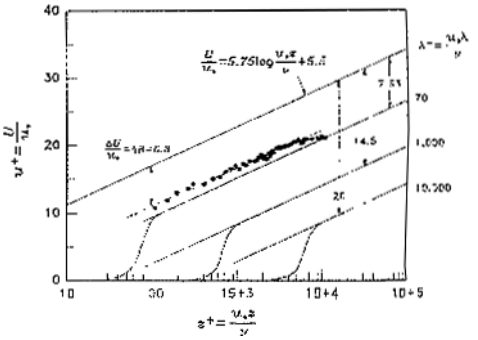

Fig. 1 Logarithmic velocity profiles on rough surfaces (*lines*, experimental data of Scholz (1955), *solid circles*, present experiments).

2. Experimental Details

The present experiments of the flow field are performed (Kim *et al.*, 1996) in the open-circuit boundary-layer wind tunnel with the contraction ratio of 3:1 and having the test section of 1.2m in width, 1.2m in height and 6m in length. A neutrally stratified atmospheric boundary layer is simulated using the equally spaced triangular spire-type vortex generators of 0.25m-height and the artificial grass.

The generated boundary layer thickness (δ) of 0.25m has a typical wind profile over open flat terrain (correspond to power-law exponent 1/7), and the gradient wind speed (U_∞) is 7m/s. Figure 1 shows the measured mean velocity profile in the inner-law coordinates (u^+, z^+) with the universal wall-law profile and the experimental data of Scholz (1955). It is well known that the rough-wall velocity profile shifts downward by an constant amount ΔB which depends upon the roughness Reynolds number λ^+. The measurements of the present experiment shows the general trend of rough-wall velocity profiles and ΔB being approximately 6.3 which corresponds to $\lambda^+ = 60$. The roughness Reynolds number $\lambda^+ = 60$ means a substantially rougher condition. The measured velocity profile is properly curve-fitted to a logarithmic law as

$$U_o(z) = \frac{u_*}{\chi} \log \frac{z}{z_o} \tag{1}$$

with the friction velocity $u_* = 0.33$m/s, the roughness height $z_o = 0.05$mm and von Kármán constant $\chi = 0.41$. The measured Reynolds stresses near the ground are $(\overline{u^2})^{1/2}/u_* = 2.3$, $(\overline{v^2})^{1/2}/u_* = 1.8$, $(\overline{w^2})^{1/2}/u_* = 1.48$ which have almost the same values of 2.5, 1.9 and 1.3 reported by Counihan (1975) for the atmospheric surface layer.

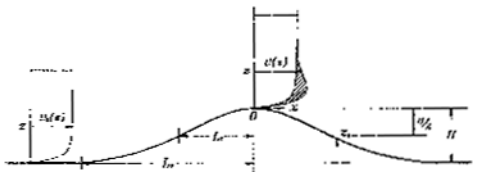

Fig. 2 Speed-up of the wind flow over a hill.

The model hills manufactured with fiber-reinforced-plastic (FRP) material have the shape of cosine-function, which is:

$$z_s(x) = \frac{H}{2}\left\{1 + \cos\left(\frac{\pi}{2} \cdot \frac{x}{L_1}\right)\right\} \tag{2}$$

Here, $z_s = 0$ for $x \geq 2L_1$ where L_1 is the upwind half length of the hill at the one-half height of the hill . The coordinate system employed in the present investigation is the right-hand Cartesian coordinate system with the origin located at the hill crest and the vertical coordinate z represents the height above the terrain surface and starts from the local elevation of the topography as shown in Fig. 2. In the figure, the schematics of speed-up characteristics due to the influence of a hill is illustrated together with the coordinate system representation.

The model hills used in the present investigation are about 1:1,000 scale models and their dimensions are listed in Table 1. The hill slope is defined as the average slope for the top half of the hill upstream of the crest, *i.e.*, $s = H/(2L_1)$.

The choice of the hill slope of 0.3 and 0.5 is based on the computational results (Kim *et al.*, 1994) which showed the flow separation in the leeside of a hill for hill slopes over 0.5 but no flow separation for the slope of 0.3. The maxi mum inclination angles of S3 and S5 hills are 25° and 38°, respectively.

The continuous double hills which are composed of two single hills of different shapes would represent more realistic hilly terrain. In the pres-

Table 1 Dimensions of two-dimensional hill models.

CASE	Slope	Hill height H[cm]	Base length $4L_1$[cm]	Re_H	δ/H
S3H4	0.3	4	26.7	1.87×10^4	6.25
S3H7		7	46.0	3.27×10^4	3.57
S3H12		12	80.0	5.60×10^4	2.08
S5H4	0.5	4	16.0	1.87×10^4	6.25
S5H7		7	28.0	3.27×10^4	3.57

* SnHm designates that the hill slope is n/10 and m is the height in centimeter.

ent work, flow characteristics of double hills S3H4-S3H7 and S5H4-S5H7 are investigated. The separation distances between the upwind hill back and the downwind hill foot are fixed to 5 cm.

The flow measurement is carried out using the standard pitot-tube and the X-type hot-wire probes (Dantec 55P61, 55P63) powered by Dantec Streamline Anemometer. From the uncertainty analysis based on Coleman and Steele (1989), the estimated maximum error for the mean velocity is 6% with the confidence level of 95%. The lateral uniformity of the flow is checked when a two-dimensional model hill is installed and found that the variations are within $\pm3\%$ of the mean velocity.

The surface static-pressure distributions are measured by a pressure transducer through pressure taps of 1mm-diameter on the hill surface and floor. The measured static pressure is represented in a non-dimensional form which is defined as

$$C_p=\frac{2(p_s-p_\infty)}{\rho U_\infty^2} \tag{3}$$

where (p_s-p_∞) is the measured static pressure difference between the hill surface and the reference upstream position, and ρ is the air density.

3. Numerical Method

The numerical method used in the present computation (Kim *et al.*, 1997a) for the solution of the Reynolds-averaged Navier-Stokes equations is based on the finite volume method in a strong conservation form and the SIMPLEC pressure correction algorithm. For the computation of the flow involving complex geometry, a non-orthogonal boundary-fitted grid system is used. The hybrid scheme is employed to discretize the convection terms in the governing equations.

For a steady-state viscous incompressible turbulent flow, the vectorized form of the governing equations in a Cartesian coordinate system are given as:

$$\boldsymbol{E}_x+\boldsymbol{F}_z=\boldsymbol{S} \tag{4}$$

where

$$\boldsymbol{E}=\begin{bmatrix}\rho U\\ \rho UU-(\mu+\mu_t)U_x\\ \rho UW-(\mu+\mu_t)W_x\\ \rho Uk-(\mu+\mu_t/\sigma_k)k_x\\ \rho U\varepsilon-(\mu+\mu_t/\sigma_\varepsilon)\varepsilon_x\end{bmatrix}$$

$$\boldsymbol{F}=\begin{bmatrix}\rho W\\ \rho WU-(\mu+\mu_t)U_z\\ \rho WW-(\mu+\mu_t)W_z\\ \rho Wk-(\mu+\mu_t/\sigma_k)k_z\\ \rho W\varepsilon-(\mu+\mu_t/\sigma_\varepsilon)\varepsilon_z\end{bmatrix} \tag{5}$$

$$\boldsymbol{S}=\begin{bmatrix}0\\ (\mu_tU_x)_x+(\mu_tW_x)_z-p_x\\ (\mu_tU_z)_x+(\mu_tW_z)_z-p_z\\ G-\rho\varepsilon-D\\ \frac{\varepsilon}{k}(C_1f_1G-C_2f_2\rho\varepsilon)+E\end{bmatrix}$$

The rate of production of turbulence kinetic energy G in the above equation is defined as

$$G=\mu_t\{2(U_x^2+W_z^2)+(W_x+U_z)^2\} \tag{6}$$

In Eqs. (4) through (6), the subscripts x and z denote partial derivatives in the respective coordinate directions, and U and W are the x and z-component mean velocities. From the eddy viscosity hypothesis, the turbulent eddy viscosity is given by

$$\mu_t=\rho C_\mu f_\mu\frac{k^2}{\varepsilon} \tag{7}$$

The standard k-ε turbulence model (Jones and Launder, 1972) contains the following empirical constants:

$$C_\mu=0.09,\ C_1=1.44,\ C_2=1.92,\quad \sigma_k=1.0,\ \sigma_\varepsilon=\frac{\chi^2}{(C_2-C_1)\sqrt{C_\mu}} \tag{8}$$

The wall-damping functions of the low-Reynolds-number model are defined as

$$f_\mu=\left\{1-\exp\left(\frac{-z^+}{26.5}\right)\right\}^2, \qquad (9)$$
$$f_1=1,\ f_2=1-0.3\exp(-Re_t^2)$$

where the local turbulent Reynolds number is defined by

$$Re_t=\frac{\rho k^2}{\mu\varepsilon} \qquad (10)$$

The extra terms for the low-Reynolds-number model are defined as

$$D=2\mu\left(\frac{\partial\sqrt{k}}{\partial z}\right)^2,$$
$$E=(1-f_\mu)\frac{2\mu\mu_t}{\rho}\left(\frac{\partial^2 U}{\partial z^2}\right)^2 \qquad (11)$$

The main difference of the low-Reynolds-number model from the standard k-ε turbulence model can be distinguished by the values of f_μ, f_1 and f_2 which assume the value of unity in the standard k-ε turbulence model. In addition, the extra terms D and E equal to zero in the standard k-ε turbulence model.

In the present computation, the low-Reynolds-number model of Nagano and Hishida (1987) is used when the flow separation occurs. Recently, Xu and Yang (1990) reviewed the low-Reynolds-number models for turbulent wall jets and reported that the Nagano-Hishida model was found most adequate. Note that the only difference between the Nagano-Hishida model and the model of Launder and Sharma (1974) is the expression of f_μ[1].

Together with the k-ε turbulence model, the modified wall function is used to consider surface roughness, which are:

$$U=\frac{u_*}{\chi}\ln\frac{z}{z_o}=\frac{u_*}{\chi}\ln(E_o z^+),$$
$$k=\frac{u_*^2}{\sqrt{C_\mu}},\quad \varepsilon=\frac{u_*^3}{\chi z} \qquad (12)$$

Here, the wall-law constant $E_o=\exp\{\chi(B-\Delta B)\}$ contains ΔB which varies by surface roughness, and the constant B is taken as 5.2. In the present computations, data of Tani (1987) is used for ΔB. In the low-Reynolds-number model, no-slip conditions for velocities and $k=\varepsilon=0$ are imposed on the ground.

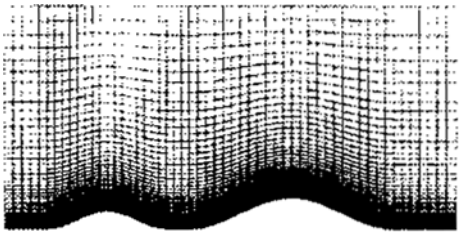

(a) Non-orthogonal grid system for the double hill, S3H4-S3H7

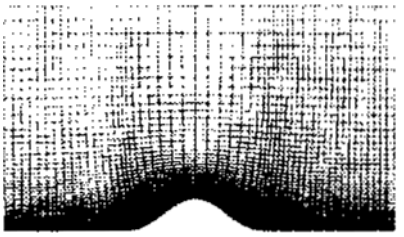

(b) Orthogonal grid system for the single hill, S5H7

Fig. 3 Schematics of the computational grid systems.

Figure 3(a) is a non-orthogonal grid system generated by an algebraic method and (b) is an orthogonal grid system by the boundary integral technique (Kang and Leal, 1992). The grid-independent solutions are obtained with (110×55) and (150×80) grid systems for the single and double hill computations, respectively. It is noted that more dense grid in wall region is required to take account of the steep change of wall-damping functions of the low-Reynolds-number model. The numerical difficulties are encountered for locating several grids within the viscous sublayer in the high Reynolds number flow where the thickness of sublayer becomes very thin. Therefore, it seems that the low-Reynolds-number model may be inappropriate for the simulation of the real atmospheric wind flow having very large Reynolds number.

The flat-floor measurements are applied as the undisturbed upstream condition. On the other boundaries except the upstream and the ground where no-slip condition is imposed, all flow

1) In the Launder-sharma model,

$$f_\mu=\exp\left(\frac{-3.4}{(1+Re_t/50)^2}\right).$$

variables are determined by extrapolation.

The concentration field is solved with the converged mean velocities and turbulent eddy viscosity. The dispersion equation for mean concentration from the gradient diffusion theory (K-theory) is written as

$$\frac{\partial C}{\partial t}+U\frac{\partial C}{\partial x_s}+W\frac{\partial C}{\partial z}=\frac{\partial}{\partial x_s}\left(K_x\frac{\partial C}{\partial x_s}\right)+\frac{\partial}{\partial z}\left(K_z\frac{\partial C}{\partial z}\right)+q(x_s, z) \quad (13)$$

where C is the mean concentration of passive scalar (non-buoyant pollutant), t is the time and $q(x_s, z)$ is the source strength function which is given as $Q\cdot\delta(0, H_s)$, where Q is the emission flow rate, H_s is the emission height and $\delta(x_s, z)$ is the Dirac delta function. Note that x_s denotes the downwind distance from the source.

The turbulent eddy diffusivities are modeled as $K_x=K_z=\nu_t/Sc_t$ where Sc_t is the turbulent Schmidt number and $Sc_t=1.0$ is used in the present calculations. The turbulent Schmidt number represents the proportionality constant between the characteristic length scale for diffusion and that for momentum transfer.

Difficulties are encountered with the gradient diffusion theory in the specification of the lateral eddy diffusivity K_y in three-dimensional dispersion, and still there are arguments for the appropriate modelling for K_y (Csanady, 1980; Galperin, 1986). In the present computations, only the two-dimensional dispersion is considered by assuming an infinite line source.

The boundary condition that applies to all boundaries is $\partial C/\partial\eta=0$, where η is the normal coordinate to the boundary surface. The converging concentration field should satisfy the following integral conservation equation:

$$\int_0^\infty U(x_s, z)\,C(x_s, z)\,dz=Q \text{ for } x_s>0 \quad (14)$$

The grid spacing is very important for an advection-diffusion problem to obtain an accurate result. In the present computation, the grid system is constructed under the guideline of Kasibhatla et al. (1988). They recommended that the time-scale ratio of turbulent diffusion to advection, $\gamma_z=K_z\Delta x/(U\Delta z^2)$, should be equal to or greater than unity to minimize numerical error. In the present calculation, the grid spacings are optimized by the following procedure: When the velocity and turbulent eddy diffusivity profiles of the boundary layer over a flat-floor are expressed as

$$U(z)=U_\infty\left(\frac{z}{\delta}\right)^a, \quad K_z(z)=\kappa u_* z/Sc_t \quad (15)$$

then, the optimized grid spacing Δz for given Δx and γ_z can be determined by

$$\Delta z^2=\left(\frac{\delta^a}{U_\infty}\frac{\kappa u_*}{Sc_t}\right)\frac{\Delta x}{\gamma_z}z^{1-a} \quad (16)$$

In the present paper, the ground-level concentration C_o is presented in a normalized form:

$$\chi_o=\frac{C_o U_\infty \delta}{Q} \quad (17)$$

where χ_o is the normalized ground-level concentration, δ the thickness of boundary layer and Q [m²/s] the emission flow rate from the line source.

4. Results and Discussion

4.1 Hypothesis of Reynolds-number independency

In most cases, the Reynolds-number similarity between the wind tunnel and the atmosphere is not attainable due to the large scale ratio. However, this does not seriously limit the possibility of modelling the atmospheric boundary-layer. The dominant flow characteristics are weakly depend upon the Reynolds number under the hypothesis of Reynolds-number independency at high Reynolds numbers. The total drag coefficient of an "aerodynamically rough" surface becomes invariant with respect to the Reynolds number (Cermak, 1984). Since essentially all natural surfaces are aerodynamically rough, the flow structure related to momentum transfer will be similar at least within the wall region, if the scaled-down roughness is not totally immersed in viscous sublayer to create an aerodynamically smoothing effect.

In the present investigation, the hypothesis of Reynolds number independency is confirmed by

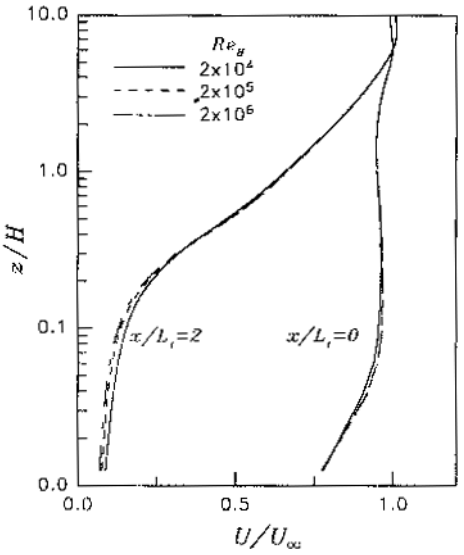

Fig. 4 Comparisons of horizontal mean velocity profile for different Reynolds numbers.

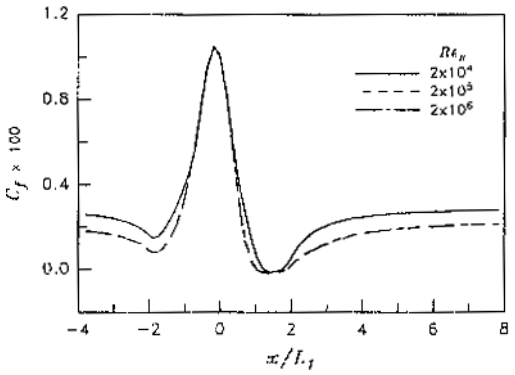

Fig. 5 Distributions of surface friction coefficient for different Reynolds numbers.

numerical simulations for the atmospheric wind flow over aerodynamically rough terrain such as a hill. Figure 4 shows the horizontal mean velocity profiles at the hill top ($x/L_1=0$) and the hill back ($x/L_1=2$) for the Reynolds numbers 2×10^4, 2×10^5 and 2×10^6. The velocity profiles are almost identical. The distributions of surface friction coefficient, C_f, is presented in Fig. 5. In the figure, C_f distributions are identical except for the case of Reynolds number 2×10^4 where the discrepancies are apparent on the upwind and downwind surface of the hill. From the results of numerical simulations, it is concluded that the

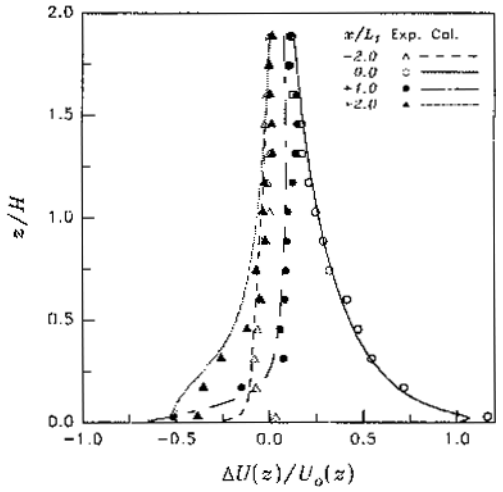

Fig. 6 Comparison of fractional speed-up ratio in S3H7 between the computation and the measurements (symbols, experiments; lines, computations).

hypothesis of Reynolds number independency is valid when the model surface is aerodynamically rough and the Reynolds number is sufficiently large, *i.e.*, over 10^4.

4.2 Wind flow over single hills

There is no flow separation in S3H4 and S3H7 as expected, but the flow separation occurs in S5H4 and S5H7. Figure 6 shows the vertical profiles of fractional speed-up ratio $\Delta S=(U(z)-U_o(z))/U_o(z)$. In the figure, it is seen that the flow is accelerated over the hill with the maximum fractional speed-up ratio of about 1.1 at the hill top and is decelerated on the downwind slope, a speed reduction is apparent at low levels. As a reference, the maximum fractional speed-up ratio by the simple approximation method by Davenport (1989) is 1.1.

Figure 7 shows the turbulence characteristic of the wind flow over the S3H7 hill. The turbulence kinetic energy is produced by the mean strain rates (mainly by $\partial U/\partial z$ and $\partial W/\partial z$ near the hill top surface, see Eq. (6)) and advected along the mean streamlines, being smoothed out by the viscous dissipation along their trajectory.

The properties of the turbulence motion carried along by the flow are strongly affected by the

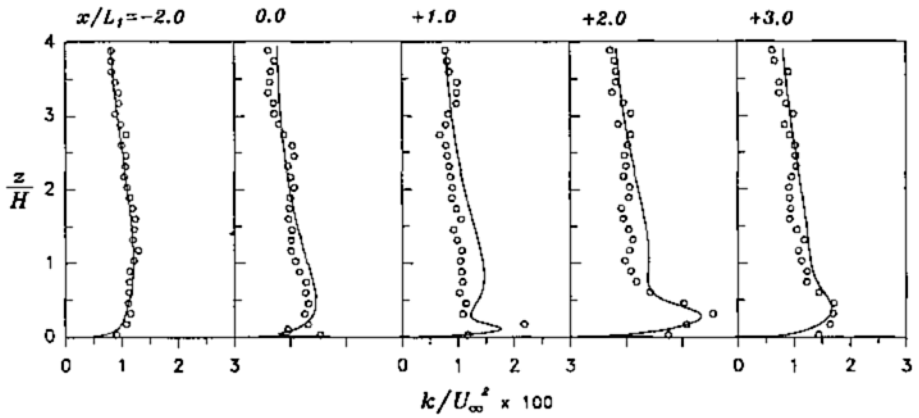

Fig. 7 Vertical profiles of turbulence kinetic energy over the single hill, S3H7 (circles, experiments; lines, computations).

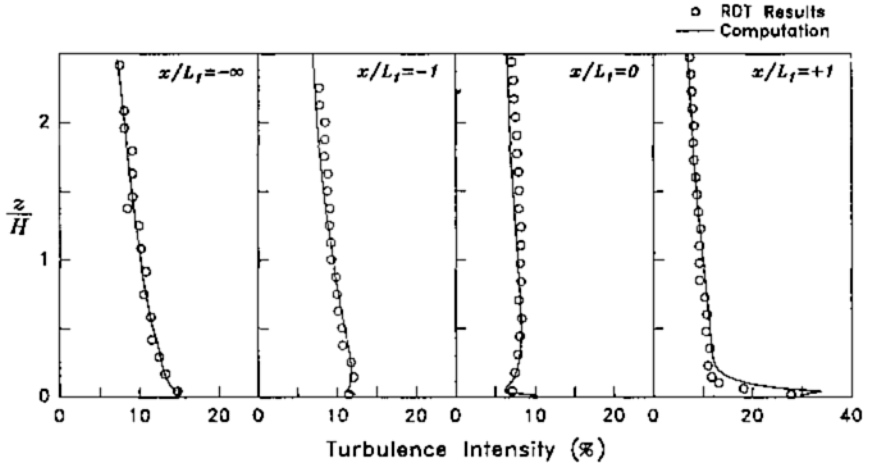

Fig. 8 Comparisons of turbulence intensity profiles between the theoretical and computational results of the single hill, S3H12 (circles, RDT predictions; lines, computations).

mean flow distortion. When the distortion produced by the mean flow is sufficiently rapid, then the turbulence kinetic energy is not significantly reduced by the viscous dissipation. Accordingly, the transformation characteristics of turbulence after the distortion can be linearly related to its upstream properties through a distortion tensor (Townsend, 1976).

For the flow over a two-dimensional hill, Newley (1985) derived the first-order equations for the change of Reynolds stresses.

$$\frac{\overline{u^2}}{\overline{u_o^2}}=1-\frac{4}{5}\frac{\Delta U(z)}{U_o}=1-\frac{4}{5}\Delta S \qquad (18)$$

where $\overline{u_o^2}$ are the Reynolds stress at the upstream.

Figure 8 presents the comparisons of turbulence intensity profiles between numerical predictions and rapid distortion theory (RDT) calculations, and the results show reasonable agreements. It is seen in the figure that the decrease in the turbulence intensity profile at all elevation on the hill crest ($x/L_1=0$) compared to the corresponding values at the other hill locations, and a large increase in the leeside surface region, *i.e.*, the wake region ($x/L_1>0$). The decreasing or increasing trend of the turbulent intensity can be interpreted by the evolution equations of the Reynolds stresses which are derived from the rapid distortion theory (see Eq. (18) in which the Reynolds stress is a function of the mean velocity

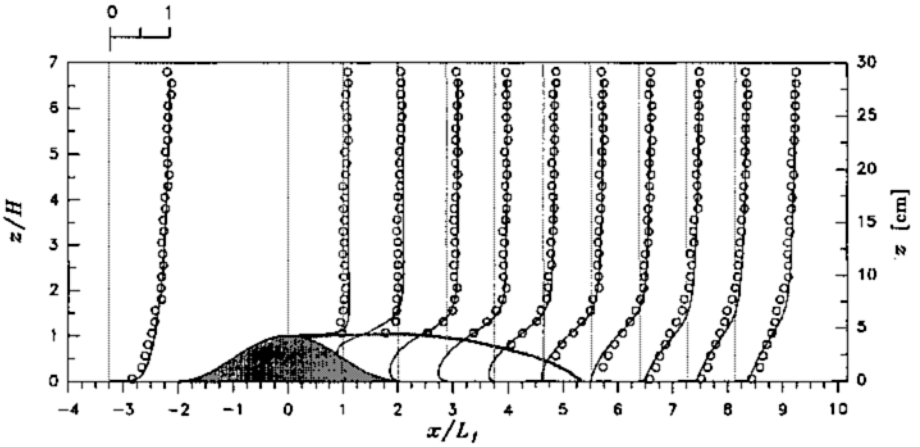

Fig. 9 Vertical profiles of mean horizontal velocity over the single hill, S5H4 (circles, experiments; lines, low-Re-number model).

perturbation, ΔU). Due to the speed-up at the hill top, the turbulence intensity decreases at all levels, and in the leeside slope, the turbulence intensity increases by the velocity deficit in the wake region. The discrepancies are found in the near-wall region where the RDT assumption is not valid.

An oil-ink dot method (Langston and Boyle, 1982) is used to find out the reattachment point in the present experiments. Figure 9 illustrates the numerical prediction of the flow over S5H4 showing the zone of flow separation. In the figure, the thick line behind the hill depicts the predicted separation region. The reattachment points obtained from the experiment and the numerical prediction are summarized in Table 2.

In the present work, the predicted length of the separation zone by the standard k-ε model is shorter than that by the low-Reynolds-number model, and this is the well known trend that the standard k-ε model with the empirical wall function does not predict the complex flow well at and beyond the flow separation. It has been reported that the low-Reynolds-number model offers better predictions in complex flows which have flow separations (Chen and Patel, 1988).

It should be noted that the recirculation zone of the present results are comparatively smaller than those created by obstructions having a sharp edge. The reattaching flow measurements for various obstructing configurations are briefly summarized in Bradshaw and Wong (1972); for example, the reattachment point of the two-dimensional fence is $x_R/H=17$, which is significantly longer than the results for the hills investigated here.

Table 2 Measured and predicted reattachment points (x_R/H).

CASE	δ/H	Experiment	Standard k-ε model	Low-Re-number model
S5H4	6.25	5.25±0.5	3.93	5.36
S5H7	3.57	4.30±0.3		5.20

* x_R is the distance between the hill top and the reattachment point.

In S5H4, the length of the separation zone from the experiment and computation (Low-Reynolds-number model) are nearly the same, but in S5H7, the computation over-predicts by about 20%. It is thought that this discrepancy is most likely caused by the limitations of the experimental set-up. The length of test section seems not long enough to ensure the independence of the recirculation zone. However, for the case of S5H4 the forementioned effect is hardly realizable because of the relatively small dimension of the model. Arya *et al.* (1987) measured the reattachment point with a similar flow condition and hill model to S5H4, and obtained $x_R/H=5.5$.

The pressure distributions on the surface are shown in Fig. 10. The measured and calculated pressure coefficients show excellent agreement in (a) S3H4 and S3H7, but discrepancies are seen in

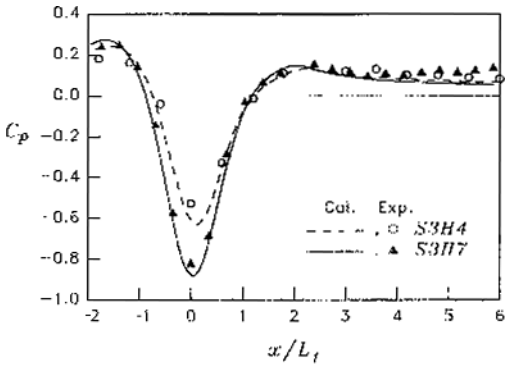

(a) S3H4 and S3H7

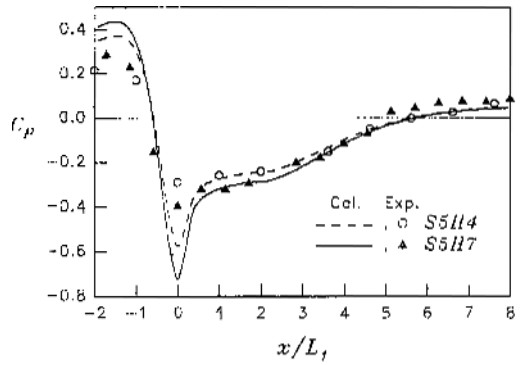

(b) S5H4 and S5H7

Fig. 10 Pressure distributions on the single hills (symbols, experiments; lines, computations).

(b) S5H4 and S5H7 where the computation predicts larger negative peak-value at the hill top.

4.3 Linear theory predictions

In the two-dimensional flow problem investigated by Jackson and Hunt (1975), the atmospheric wind flow over a gently sloped low hill is divided into two regions: the inner layer and outer layer. In the outer inviscid flow region, the mean velocity perturbation is governed by the dynamic pressure perturbation caused by a hill. The inner layer is the thin layer of thickness l on the ground and within which shear stress plays a dominant role to determine the mean velocity.

The linear theory of Jackson and Hunt predicts that the maximum speed-up at the hill top occurs at the height of inner layer length scale l which is defined as

Table 3 The inner layer length scale from theory and computation.

Hill heigh	Hill length	Jackson & Hunt	Mason	Computation
$H[cm]$	$4L_1[cm]$	$l[mm]$	$l^*[mm]$	$l^c[mm]$
4.0	26.7	4.9	1.8	2.0
7.0	46.0	7.7	2.5	3.5
12.0	80.0	12.1	3.7	7.0

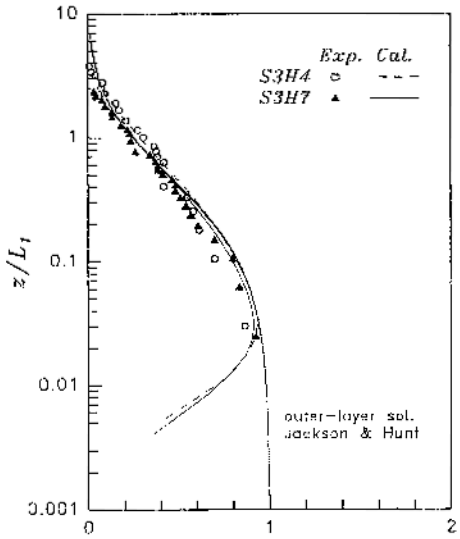

Fig. 11 Comparison of the non-dimensional speed-up profiles at the hill top between the theoretical prediction and the present results (symbols, experiments; lines, computations).

$$l \cdot \ln(l/z_0) = 2\kappa^2 L_1 \tag{19}$$

Later, Mason (1986) has pointed out that the inner layer length scale of Jackson and Hunt may be inappropriate, and suggested an alternative inner layer length scale l^* by

$$l^* \cdot \ln^2(l^*/z_0) = 2\kappa^2 L_1 \tag{20}$$

The inner layer heights of the present computation, which are presumed to be the height where the maximum non-dimensional speed-up occurs, are compared with those of the linear theory in Table 3.

It is obvious that the inner layer length scale of Mason gives closer value to the present computation. Figure 11 presents the non-dimensional

speed-up velocity profile $\sigma(z)$ above the hill top. The agreement between the present results and the outer-layer solution of Jackson and Hunt is excellent, but it should be noted that S3Hm hills are the gently sloped low hills without flow separation.

4.4 Wind flow over double hills

Figure 12 presents the profiles of mean velocity for the double hill configurations of (a) S3H4 -S3H7 and (b) S5H4-S5H7. The comparisons between the prediction and the experimental results are in reasonable agreement. The size of the separation region at the leeside of the second hill is decreased from that of the single hill by about 20%. It is considered that increased turbulence kinetic energy during the passage of the flow over hills makes the second separation region smaller than that of the single hill (Armaly *et al.*, 1983). This trend is also reported by Ferreira *et al.* (1991). The experimental and numerical results of the wind flow over the double hills S3H7-S3H4 and S5H7-S5H4 can be found in Kim *et al.* (1997b).

As shown in Fig. 13, pressure distributions of double hills with hill slopes of 0.3 are not so much changed as those of single hills. The same negative peak values appear at the hill tops and the similar patterns prevail.

4.5 Dispersion over the flat-floor

In order to compare with the dispersion over double hills and to validate the accuracy of numerical prediction, the dispersion over the flat

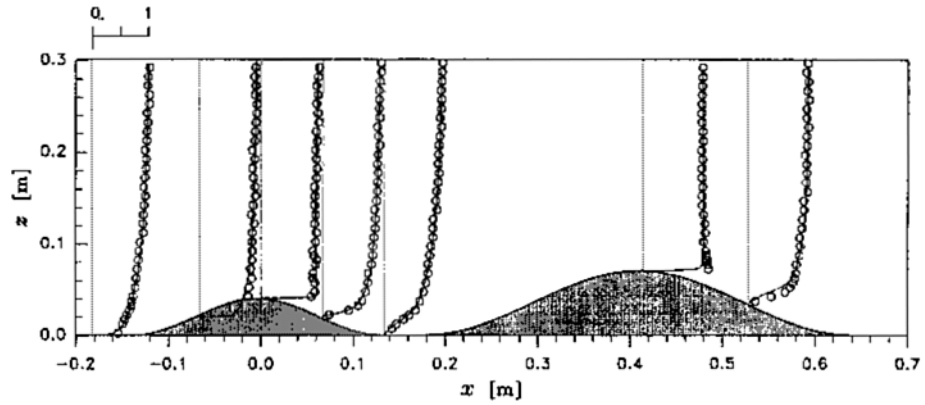

(a) S3H4-S3H7 (k-ε turbulence model)

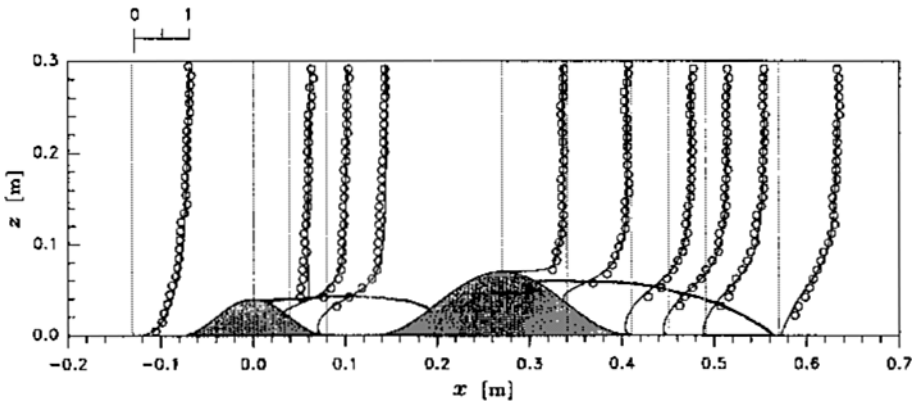

(b) S5H4-S5H7 (low-Re-number model)

Fig. 12 Vertical profiles of mean horizontal velocity over the double hills (circles, experiments; lines, computations).

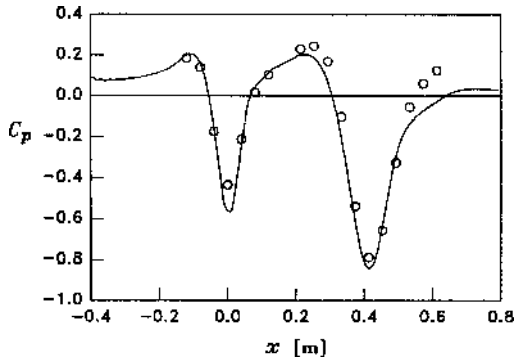

Fig. 13 Pressure distributions on the double hill, S3H4-S3H7 (circles, experiments; lines, computations).

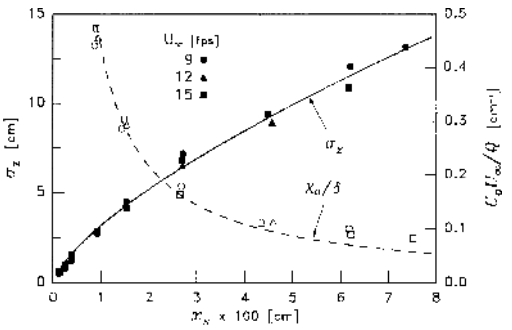

Fig. 14 Vertical plume half-width and ground-level concentration in the flat-floor from the ground-level line source (symbols, experiments of Poreh and Cermak (1964); lines, computations).

-floor is calculated. Figure 14 shows good agreements between the computation and the experiments of Poreh and Cermak (1964) for the dispersion from a ground-level line source in flat floor. In the figure, σ_z denotes the vertical plume half-width which is the distance at which the maximum concentration falls to half its value, and C_o is the ground-level concentration (GLC). Figure 15 shows the comparison of mean concentration profiles between the computed results and the measured results of Raupach and Legg (1983) for the dispersion from an elevated line source in flat -floor. Generally, the computation well predicts the measured mean concentrations except in the close vicinity of the source where the computation under-estimates the peak value as shown in Fig. 15 at $x_s/H_s=2.5$. This trend is consistent with the well-known failure of the gradient diffusion theory close to a source in a turbulent flow. The analytical solution from the gradient diffusion theory (Rounds, 1955) gives the peak value $\chi_s=1.40$ at $x_s/H_s=2.5$ while the computation predicts the close value, $\chi_s=1.35$. Another possible reason of this discrepancy can be found in the usage of a finite-volume source instead of a point source. The numerical method used in the present computation is based on the finite-volume discretization so that a point source is modeled as a finite -volume source. Karamchandani *et al.* (1983) have pointed that the concentration in the close vicinity of a source is underestimated when a point source is replaced by a finite volume source.

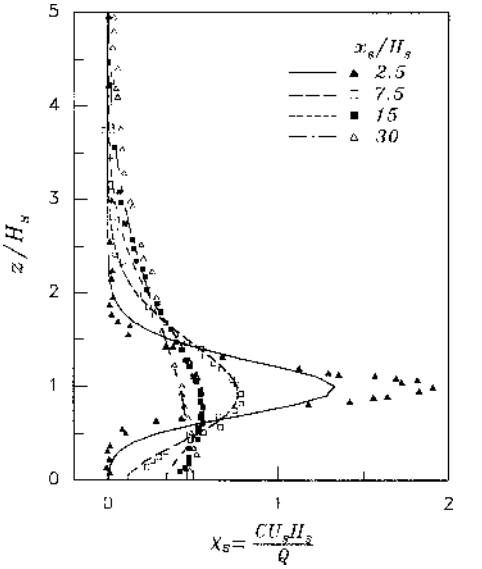

Fig. 15 Mean concentration profiles in the flat-floor from the elevated line source (symbols, experiments of Raupach and Legg (1983); lines, computations).

As references, the dispersion over a flat-floor is calculated and compared with the analytical solutions. In Fig. 16, the GLC distributions are fitted reasonably well with the analytical solution of Huang (1979) when the results are normalized with the distance x_m at which the maximum GLC occurs, C_o with the emission height H_s, and the wind velocity at the emission height U_s. Figure 17 shows the variations of the vertical plume half

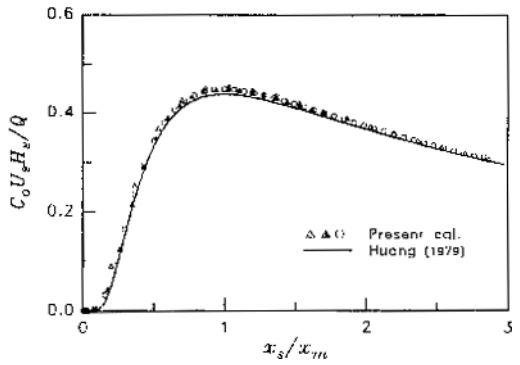

Fig. 16 Normalized ground-level concentrations in the flat-floor from the elevated line source (symbols, computations; lines, analytical solutions).

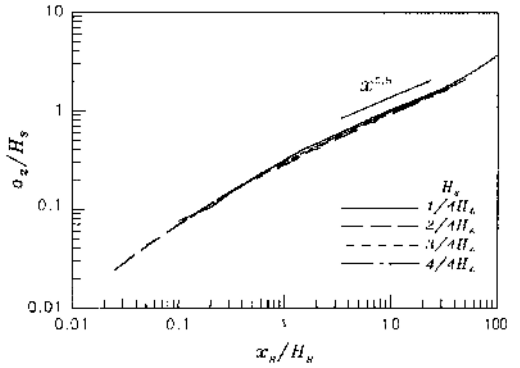

Fig. 17 Variations of vertical plume half-width with respect to the normalized downstream distance for different emission heights.

-width which increases proportionally to $x_s^{1/2}$ far downstream from the source. In the statistical theory of turbulence diffusion (Batchelor, 1949), the turbulent eddy

diffusivity can be related to the plume half-width as

$$K_z=\frac{1}{2}\frac{d\sigma_z^2}{dt}=\frac{U_s}{2}\frac{d\sigma_z^2}{dx_s} \tag{21}$$

where the Lagrangian description is transformed into the Eulerian form by the hypothesis of 'frozen' turbulence. It can be deduced that $\sigma_s\sim x_s^{1/2}$ if the turbulent eddy diffusivity of a flat-floor boundary layer is approximated as $K_z=\kappa u_* z/Sc_t\neq f(x_s)$.

4.6 Dispersion over double hills

Figure 18 depicts the distributions of GLC from the sources located at the upstream base with heights of 1/4 H_4, 2/4 H_4, 3/4 H_4 and 4/4 H_4, where H_4 is the hill height of SnH4. The GLC decreases sharply with increasing emission height. In (a) S3H4-S3H7, the distribution shapes and maxima of GLC are not so different from those of the flat-floor dispersion whereas significant changes are seen in (b) S5H4-S5H7 and this is mainly due to flow separations.

Figure 19 represents the vertical profiles of mean concentration for S3H4-S3H7 and S5H4-S5H7, and significant differences (far from reflected Gaussian) are found at the valley and second hill back where the recirculation regions exist. The concentration levels within separation regions are constant and its profiles are far from Gaussian due to the strong turbulence mixing and this trend is obvious in Figs. 18 (b) and 19.

The most critical location of the source which leads to maximum GLC is at or near the downwind base of the hill. Figure 20 illustrates the GLC distributions when the source is located at the valley. In (a) S5H4-S5H7, the source is located within the separation zone so that the concentration levels in that region are high because the plume is trapped in the recirculation zone. If the source is close to the ground, as shown in Fig. 20 (b), the maximum value of GLC occurs upstream of the source, as pollutant is accumulated through upstream convection to the base of the hill; the same phenomena was observed by Arya *et al.* (1981).

The source located within a recirculation region gives rise to much enhanced GLC near the source due to the presence of the hill, but significantly reduced GLC far from the source or the hills. This is probably due to the rapid diffusion by considerably enhanced turbulence within a separation zone, resulting in significantly increasing GLC near the valley and decreasing GLC farther downstream.

Terrain amplification factor (TAF) which is the ratio of maximum GLC in the presence and absence of hills for the same source strength and height is given in Table 4. TAF is a simple

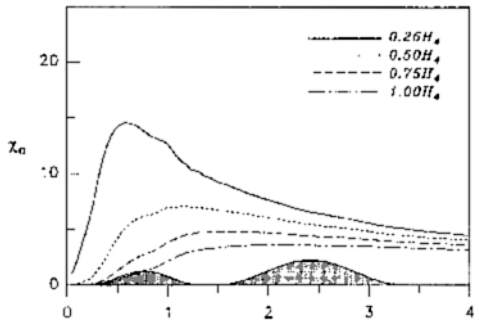

(a) S3H4-S3H7

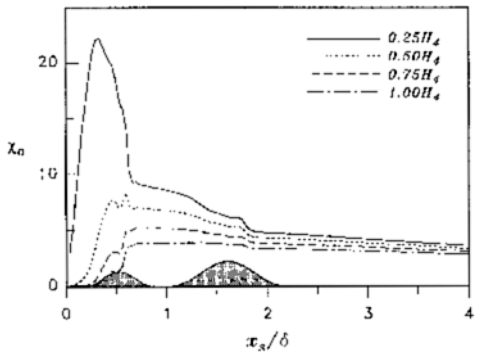

(b) S5H4-S5H7

Fig. 18 Distributions of ground-level concentration over the double hills from the elevated line source at upwind base.

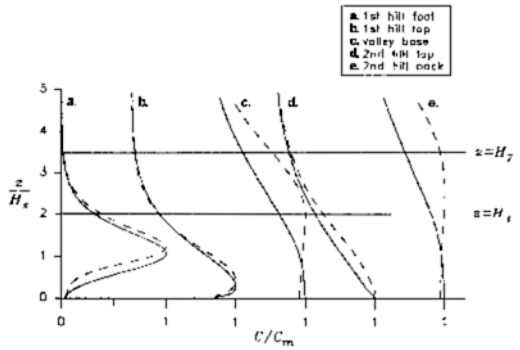

Fig. 19 Comparison of mean concentration vertical profiles over the double hills from the source at upwind base with the emission height $H_s = 0.5H_4$ (solid lines, S3H4-S3H7; dashed lines, S5H4-S5H7).

measure of the topographic effect on peak GLC which is the primary concern for environmental assessment. Values of TAF much larger than unity are obtained for sources located at the

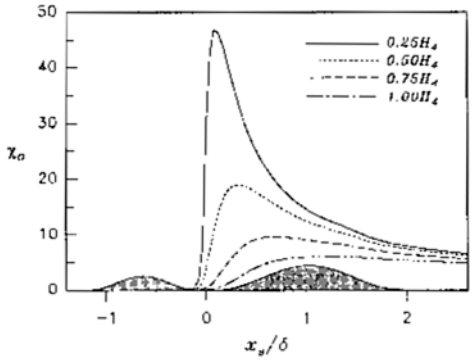

(a) S3H4-S3H7

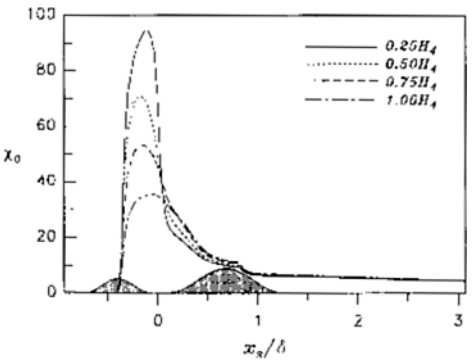

(b) S5H4-S5H7

Fig. 20 Distributions of ground-level concentration over the double hills from the elevated line source at valley base.

Table 4 Terrain amplification factors for double hills.

Source height H_s/H_4	S3H4-S3H7		S5H4-S5H7	
	Source at upwind base	Source at valley	Source at upwind base	Source at valley
0.25	0.84	2.70	1.28	5.45
0.50	0.93	2.51	1.10	9.33
0.75	1.01	2.05	1.11	11.28
1.00	1.06	1.77	1.15	10.47

downwind base of the hill (valley) while for sources located at the upwind base and relatively low heights ($H_S = 0.25H_4$), TAFs are less than unity.

4.6 Dispersion from a temporally released source

The influence of topography on the dispersion

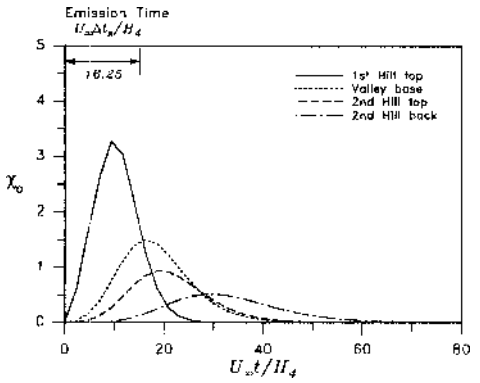

(a) S3H4-S3H7

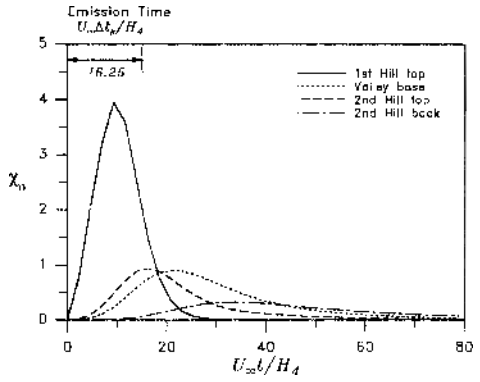

(b) S5H4-S5H7

Fig. 21 Histories of ground-level concentration from the temporally released source at upwind base with the emission height $H_s = 0.25\ H_4$.

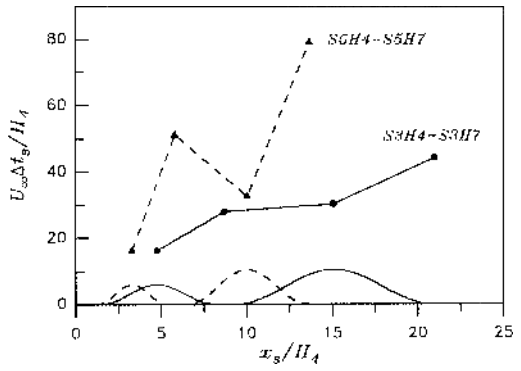

Fig. 22 Comparisons of duration time for the double hills from the temporally released source at upwind base.

from a temporally released source may be more severe than that from a continuous source. However, experimental simulation for the transient dispersion is very difficult because of the limitations of measurements.

Figure 21 shows GLC variations of several positions with respect to time. It is interesting to note that GLC at the second hill top grows ahead of that at the valley, although the second hill top is located at downstream of the valley. The plume core convected along the separated streamline from the first hill top impacts on the second hill top, and then the plume starts to diffuse in the valley by recirculating flow.

Figure 22 represents the time Δt_s, which is the duration time of positive GLC. It can be interpreted that the duration time is the period during which the pollutants prevails. The duration times in separation regions of S5H4-S5H7 are apparently longer while those at the first and second hill tops of S5H4-S5H7 are nearly equal to those of S3H4-S3H7.

5. Conclusions

The present investigation presents the numerical predictions of the wind flow and concentration field over two-dimensional hilly terrain. The results include comparisons between the computational and the experimental results of the flow fields over two-dimensional single and double hills having hill slope of 0.3 and 0.5. It is checked that the standard k-ε model is reasonably accurate in predicting the attached flow, while the low-Reynolds-number model is more suitable to simulate the separated flows. The maximum GLC decreases with increasing emission height for all cases. As a result, the worst location of the pollutant source, in the viewpoint of maximum GLC, is at or near the downwind base of the hill; especially, the worse situation arises when the source is located within separation zones.

Acknowledgment

The present investigation was carried out as a part of the project of the Environmental Fluid Mechanics Group of Advanced Fluid Engineering Research Center of Pohang University of

Science and Technology. The project was supported by Korea Science and Engineering Foundation.

References

Armaly, B. F., Durst, F., Pereira, J. C. F. and Schönung, B., 1983, "Experimental and Theoretical Investigation of Backward-Facing Step Flow," *J. Fluid Mech.*, Vol. 127, pp. 473~496.

Arya, S. P. S., Shipman, M. S. and Courtney, L. Y., 1981, "An Experimental Investigation of Flow and Diffusion in the Disturbed Boundary Layer Over a Ridge: II. Diffusion From a Continuous Point Source," *Atmos. Environ.*, Vol. 15, No. 7, pp. 1185~1194.

Arya, S. P. S., Capuano, M. E. and Fagen, L. C., 1987, "Some Fluid Modeling Studies of Flow and Dispersion Over Two-Dimensional Low Hills," *Atmos. Environ.*, Vol. 21, No. 4, pp. 753~764.

Bradshaw, P. and Wong, F. Y. F., 1972, "The Reattachment and Relaxation of a Turbulent Shear Layer," *J. Fluid Mech.*, Vol. 52, Pt. 1, pp. 113~135.

Cermak, J. E., 1984, "Physical Modelling of Flow and Dispersion Over Complex Terrain," *Boundary-Layer Meteorol.*, Vol. 30, pp. 261~292.

Chen, H. C. and Patel, V. C., 1988, "Near-Wall Turbulence Models for Complex Flows Including Separation," *AIAA J.*, Vol. 26, No. 6, pp. 641~648.

Coleman, H. W. and Steele, W. G., 1989, *Experimentation and Uncertainty Analysis for Engineers*, John Wiley & Sons., 205 pp.

Counihan, J., 1975, "Adiabatic Atmospheric Boundary Layers: A Review and Analysis of Data from the Period 1880-1972," *Atmos. Environ.*, Vol. 9, pp. 871~905.

Crooks, G. and Ramsay, S., 1993, "A Wind Tunnel Study of Mean and Fluctuating Concentrations in a Plume Dispersion Over a Two-Dimensional Hill," *Boundary-Layer Meteorol.*, Vol. 66, pp. 155~172.

Csanady, G. T., 1980, *Turbulent Diffusion in the Environment*, D. Reidel Publishing Co., Netherland, p. 249.

Davenport, A. G., 1989, "Proposed New International (ISO) Wind Load Standard," Recent Advances in Wind Engineering: *Proc. of the 2nd Asia-Pacific Symposium on Wind Engineering*, Beijing, China, Sun, T. F., Ed., Vol. II, pp. 1199~1214.

Ferreira, A. D., Silva, M. C. G., Viegas, D. X. and Lopes, A. G., 1991, "Wind Tunnel Simulation of the Flow Around Two-Dimensional Hills," *J. Wind Eng. Ind. Aerodyn.*, Vol. 38, pp. 109~122.

Galperin, G., 1986, "A Modified Turbulent Energy Model for Diffusion from Elevated and Ground Point Sources in Neutral Boundary Layers," *Boundary-Layer Meteorol.*, Vol. 37, pp. 245~262.

Glekas, J. P. and Bergeles, G. C., 1994, "Dispersion Under Neutral Atmospheric Conditions," *Int. J. Numer. Methods Fluids*, Vol. 19, pp. 237~257.

Gong, W., 1991, "A Wind Tunnel Study of Turbulent Dispersion Over Two- and Three-Dimensional Gentle Hills From Upwind Point Sources in Neutral Flow," *Boundary-Layer Meteorol.*, Vol. 54, pp. 211~230.

Huang, C. H., 1979, "A Theory of Dispersion in Turbulent Shear Flow," *Atmos. Environ.*, Vol. 13, pp. 453~463.

Jackson, P. S. and Hunt, J. C. R., 1975, "Turbulent Wind Flow Over a Low Hill," *Quart. J. Roy. Meteorol. Soc.*, Vol. 101, pp. 929~955.

Jones, W. P. and Launder, B. E., 1972, "The Prediction of Laminarization with a Two-Equation Model of Turbulence," *Int. J. Heat Mass Transfer*, Vol. 15, pp. 301~314.

Kang, I. S. and Leal, L. G., 1992, "Orthogonal Grid Generation in a 2D Domain via the Boundary Integral Technique," *J. Comput. Phys.*, Vol. 102, pp. 78~87.

Karamchandani, P. and Peters, L. K., 1983, "Analysis of the Error Associated with Grid Representation of Point Sources," *Atmos. Environ.*, Vol. 17, No. 5, pp. 927~933.

Kasibhatla, P. S., Peters, L. K. and Fairweather, G., 1988, "Numerical Simulation of Transport from an Infinite Line Source: Error

Analysis," *Atmos. Environ.,* Vol. 22, No. 1, pp. 75 ~82.

Kim, H. G., Kyong, N. H. and Lee, C. M., 1994, "Numerical Analysis of the Flow Over a Hill," *Proc. of Spring Meeting, KSME, Taejeon,* Vol. II, pp. 223~238.

Kim, H. G., Lee, C. M., Lim, H. C. and Kyong, N. H., 1996, "Theoretical, Experimental and Numerical Study on the Atmospheric Flow Over a Hill," *Proc. of Spring Meeting, KSME, Pusan,* Vol. B, pp. 258~263.

Kim, H. G., Lee, C. M. and Kyong, N. H., 1997a, "Numerical Study on the Wind Flow Over Hilly Terrain," *J. Korea Air Pollution Research Association,* Vol. 13, No. 1, pp. 65~77.

Kim, H. G., Lee, C. M., Lim, H. C. and Kyong, N. H. (1997b) "An Experimental and Numerical Study on the Flow Over Two-Dimensional Hills," *J. Wind Eng. Ind. Aerodyn.,* Vol. 66, pp. 17~33.

Langston, L. S. and Boyle, M. T., 1982, "A New Surface-Streamline Flow-Visualization Technique," *J. Fluid Mech.,* Vol. 125, pp. 53~58.

Launder, B. E. and Sharma, B. T., 1974, "Application of the Energy Dissipation Model of Turbulence to the Calculation of Flow Near a Spinning Disc," *Lett. Heat Mass Transfer,* Vol. 1, pp. 131~138.

Ma, J. and Robson, R. E., 1995, "Turbulent Dispersion of Pollutant Over Complex Terrain," *Earth, Moon and Planets,* Vol. 72, pp. 149~175.

Mason, P. J., 1986, "Flow Over the Summit of an Isolated Hill," *Boundary-Layer Meteorol.,* Vol. 37, pp. 385~405.

Mouzakis, F. N. and Bergeles, G. C., 1991, "Numerical Prediction of Turbulent Flow Over a Two-Dimensional Ridge," *Int. J. Numer. Methods Fluids,* Vol. 12, pp. 287~296.

Nagano, Y. and Hishida, M., 1987, "Improved Form of the k-ε Model for Wall Turbulent Shear Flows," *J. Fluids Eng.,* Vol. 109, pp. 156~160.

Newley, T. M. J., 1985, Turbulent Air Flow Over Hills, Ph. D. Thesis, University of Cambridge.

Ohba, R., Ukeguchi, N., Kakishima, S. and Lamb, B., 1990, "Wind Tunnel Experiment of Gas Diffusion in Stably Stratified Flow Over a Complex Terrain," *Atmos. Environ.,* Vol. 24A, No. 8, pp. 1987~2001.

Poreh, M. and Cermak, J. E., 1964, "Study of Diffusion from a Line Source in a Turbulent Boundary Layer," *Int. J. Heat Mass Transfer,* Vol. 7, pp. 1083~1095.

Raupach, M. R. and Legg, B. J., 1983, "Turbulent Dispersion from an Elevated Line Source: Measurements of Wind-Concentration Moments and Budgets," *J. Fluid Mech.,* Vol. 136, pp. 111 ~137.

Rounds, W., 1955, "Solutions of the Two -Dimensional Diffusion Equations," *Trans. Amer. Geophys. Union,* Vol. 36, No. 2, pp. 395 ~405.

Snyder, W. H., Khurshudyan, L. H., Nekrasov, I. V., Lawson, R. E. and Thompson, R. S., 1991, "Flow and Dispersion of Pollutants Within Two -Dimensional Valleys," *Atmos. Environ.,* Vol. 25A, No. 7, pp. 1347~1375.

Tani, I., 1987, *Turbulent Boundary Layer Development Over Rough Surface,* Perspectives in Turbulence Studies, Meier, H. U. and Bradshaw, P., Eds., Springer.

Townsend, A. A., 1976, *The Structure of Turbulent Shear Flow,* Cambridge University Press, Cambridge, 158 pp.

Xu, X. F. and Yang, K. T., 1990, "Prediction of Low Reynolds Number Turbulent Wall Jets and Plumes With and Without Buoyancy," *Proc. of the 9th Int. Heat Transfer Conf.,* Hemisphere, Washington, DC, pp. 155~160.